Autophagy inhibition blunts PDGFRA adipose progenitors' cell-autonomous fibrogenic response to high-fat diet

Geneviève Marcelin, Carla da Cunha, Camille Gamblin, Nadine Suffee, Christine Rouault, Arnaud Leclerc, Amélie Lacombe, Nataliya Sokolovska, Emmanuel Gautier, Karine Clément, et al.

Autophagy inhibition blunts PDGFRα adipose progenitors' cell-autonomous fibrogenic response to high fat diet Manuscript -with full author details

Geneviève Marcelin, Carla Da, Cunha 1&, Camille Gamblin, Nadine Suffee, Christine Rouault, Arnaud Leclerc, Amélie Lacombe, Nataliya Sokolovska, Emmanuel Gautier, et al.

Autophagy inhibition blunts PDGFRα adipose progenitors' cell-autonomous fibrogenic response to high fat diet

Running head: progenitor autophagy inhibition blunts adipose tissue fibrosis.

Article type : research paper.

Authors names:

Genevieve Marcelin[1&], Carla Da Cunha[1&], Camille Gamblin[1], Nadine Suffee[2], Christine Rouault[1], Arnaud Leclerc[1], Amelie Lacombe[3], Nataliya Sokolovska[1], Emmanuel L, Gautier[2], Karine Clément[1,4] and Isabelle Dugail[1*]

Affiliations :

[1] Sorbonne Université, INSERM, UMR1269 Nutrition and Obesities, systemic approaches (NutriOmics), Paris, France;

[2] INSERM, Sorbonne Université, U1166, Paris, France;

[3] Institute of Cardiometabolism and Nutrition (ICAN), Paris, France;

[4] Asssistance Publique-Hôpitaux de Paris, Pitié-Salpêtrière hospital, Nutrition department, Paris, France.

[&]equally contributed

* Corresponding author: isabelle.dugail@inserm.fr

Corresponding adress : UMR 1269, Faculté de médecine Pitié-Salpêtrière,

91 bd de l'hôpital, 75013 Paris, France. Phone : + 33 140779730

Abstract:

Adipose tissue (AT) fibrosis in obesity compromises adipocyte functions and responses to intervention induced-weight loss. It is driven by AT progenitors with dual fibro/adipogenic potential, but pro-fibrogenic pathways activated in obesity remain to be deciphered. To investigate the role of macroautophagy/autophagy in AT fibrogenesis, we used *Pdgfra-Cre*^{Ert2} transgenic mice to create conditional deletion of *Atg7* alleles in AT progenitor cells (*Atg7* cKO) and examined sex-dependent, depot-specific AT remodeling in high-fat diet (HFD)-fed mice. *Atg7* cKO mice had markedly decreased extracellular matrix (ECM) gene expression in visceral, subcutaneous and epicardial adipose depots compared to *Atg7*$^{lox/lox}$ littermates. ECM gene program regulation by autophagy inhibition occurred independently of changes in the mass of fat tissues or adipocyte numbers of specific depots, and could be mimicked in cultured preadipocytes treated with pharmacological or siRNA-mediated autophagy disruptors. We found that autophagy inhibition promotes global cell-autonomous remodeling of the paracrine TGF-BMP family landscape, whereas ECM gene modulation was independent of the autophagic regulation of GTF2IRD1. The progenitor-specific mouse model of Atg7 inhibition confirms requirement of autophagy for white/beige adipocyte turnover, and combined to *in vitro* experiments, reveal progenitor autophagy dependence for AT fibrogenic response to HFD, through paracrine remodeling of TGF-BMP factors balance.

List of abbreviations:

CQ: chloroquine; ECM: extracellular matrix; EpiAT: epididymal adipose tissue; GTF2IRD1: general transcription factor II I repeat domain-containing 1; HFD: high-fat diet; KO: knockout; OvAT: ovarian adipose tissue; PDGFR: platelet derived growth factor receptor; ScAT: subcutaneous adipose tissue; TGF-BMP: transfrorming growth factor-bone morphogenic protein.

Key words: Atg7, chloroquine, collagen, extracellular matrix, fibrosis, obesity, subcutaneous adipose tissue,

Introduction

In obesity, chronic energy excess results in fat mass accumulation via enlargement of existing adipocytes and recruitment of progenitors to generate new fat cells [1]. The adipose tissue microenvironment is concomitantly impacted, as the network of blood vessels in the vicinity of which progenitors reside also expands [2] and resident immune cells become polarized towards a pro-inflammatory phenotype [3]. Chronically, adipose tissue (AT) low grade inflammation is highly connected to the deterioration of metabolic health and is frequently observed along with tissue fibrosis, which is defined by the accumulation of excessive extracellular matrix (ECM) and stiffness [4]. AT fibrosis ultimately compromises adipose tissue metabolic flexibility as well as whole body homeostasis, and negatively predicts response to weight loss interventions [5, 6].

Central to the development of adipose tissue fibrosis is a progenitor cell population positive for PDGFRα/Pdgfrα (platelet derived growth factor receptor, alpha polypeptide) expression, which was recently defined as a reservoir for fibroblast activation [7-9]. PDGFRα cells can also differentiate into new adipocytes with a white (fat storing) or a beige (with inducible thermogenic activity) phenotype [10 ,11]. Thus, due to their dual potential towards adipocyte or fibroblast differentiation, they are referred to as fibro/adipogenic progenitors. Beyond formation of anatomically defined fat pads, PDGFRα^{+} progenitors also govern fat cell deposition in other organs such as the heart, in particular the cardiac atria, by supporting adipocyte formation and epicardial lipid accumulation [12].

How obesity-related AT fibrosis develops is still poorly understood, in spite of its adverse consequence on AT flexibility (i.e. energy-dependent switches in repeated

states of expansion and shrinkage) which limits weight loss outcomes to bariatric surgery treatment. Recent work from our team identified a progenitor subclass marked by CD9 surface expression in mice and humans, which is associated with the production of fibrosis in visceral AT [9]. Inflammation and particularly TLR4 activation, a hallmark of the obese AT micro-environment perturbation, was also shown to contribute to obesity-induced fibrosis in mice [13]. Finally, because alternatively activated macrophages (M2-like) participate in extracellular collagen degradation through a mannose receptor phagocytic pathway [14], altered balance in M2/M1 macrophage polarization in obesity is likely to favor extracellular matrix accumulation in the long term, due to lack of clearance of extracellular material.

Plasticity in fates of fibro/adipose cells was recently reported in the hair follicle niche where fat cells could regenerate from myofibroblasts after wound healing [15]. AT fibrogenic response might thus result from a progenitor switch driven by factors in the tissue microenvironment. To investigate the functional pathways governing this switch, we manipulated the autophagy pathway, which is key in cell fate determination. Pioneer electron microscopy studies of 3T3-L1 cells identified autophagy as a crucial morphological episode in cytoplasm/organelle transformation during adipocyte conversion [16], and later studies on fat cell formation have described reciprocal relationship between autophagy and ciliogenesis [17], disrupted in rare forms of obesity presenting with ciliopathies. Accordingly, genetic mice models with adipocyte-specific autophagy deficiency produce lean animals with impaired fat cell development [18].

We here created a mouse model of conditional autophagy inhibition in adipose progenitors by inactivating *Atg7* in cells expressing inducible Cre recombinase under the control of a *Pdgfra* gene promoter, and explored AT of these animals under

obesogenic conditions. We found that autophagy inhibition in progenitors strongly attenuated AT fibrogenic response to high fat diet (HFD). In several fat depots including the pericardial cell layer of the atria, fibrogenic and ECM program was highly impaired in mice with autophagy deficiency. Mechanistically, we show that autophagy inhibition triggers a cell-autonomous fibrogenic impairment, linked to profound remodeling the Tgf-Bmp signaling gene program.

Results

Depot- and Sex- dependent efficiency of a Pdgfrα *promoter to target AT progenitors autophagy.*

PDGFRα expression is a well-established feature of AT progenitors (Fig. 1A), but there is controversy on the efficiency of the PDGFRα-Cre model to target adipose tissue precursors in studies using male mice [19,10]. Considering female as well as male mice, we have used a floxed fluorescent reporter to assess its effectiveness in FACS-purified progenitor populations from high-fat diet-fed animals (Fig. 1B). We observed that Cre-mediated gene deletion occurred in female Subcutaneous AT (ScAT) with the highest frequency (76%), but was not detectable in periovarian AT (OvAT). In males, we found that approximately 40% of progenitors recombined in ScAT or visceral Epidydimal AT (EpiAT). To inhibit autophagy, we selected *Atg7* as a target gene, because i) Cre recombinase activity at the *Atg7* locus was used in several studies using different tissue specific promoters [18, 20-22] and ii) in previous analysis of FACS sorted PDGFRα+ progenitors isolated from fibrosis-proned AT of C3H/HeOuJ mice strain fed a HFD that had acquired a myofibroblastic phenotype [9], *Atg7* was the most strongly induced among a set of autophagy-related genes in HFD mice (Fig; 1C). Mice homozygous for a floxed exon 14 at the *Atg7* locus were cross-bred with PDGFRα-Cre^{Ert2} transgenic animals, all on a pure C57/Bl6 genetic background, to produce

Atg7$^{lox/lox}$ and *Atg7*$^{lox/lox}$*-PDGFRα-Cre*^{Ert2} littermates that were treated with tamoxifen post-weaning for 5 days to induce *Atg7* inhibition in recombinase expressing cells, before shifting to HFD. As expected, qPCR analysis of *Atg7* mRNA indicated unaffected expression in AT macrophages but specific reduction in FACS sorted AT PDGFRα+ progenitors of Cre+ versus Cre- animals (Fig. 1D). In agreement with the monitoring of Cre mediated recombination in Fig. 1B, we found that approximately 50% of Atg7 mRNA was ablated in subcutaneous or male visceral AT, and confirmed that only 20% of progenitor *Atg7* expression could be targeted in the visceral fat of female mice. In agreement with efficient recombination in subcutaneous fat of female mice, reduction of Atg7 protein content is detected in ScAT of *Atg7*$^{lox/lox}$*-PDGFRα-Cre* female mice without a need of tissue fractionation (Fig. 1E), accompanied by decreased LC3-II lipidated form, a marker of autophagosome density downstream of Atg7 (Fig. 1E-F), indicating disrupted autophagy. Thus, in our hands (i.e mice maintained under obesogenic high fat diet), PDGFRα promoter-driven gene recombination can target progenitors although in a depot- and sex-specific manner. As recombination was poorly efficient in periovarian depots of female mice, subsequent experiments excluded this particular fat pad in AT phenotyping.

Atg7 deficiency in adipose tissue progenitors attenuates HFD-induced fibrogenic programming.

After 10 weeks on HFD, mice adipose tissue morphology was examined by immunostaining of paraffin-embedded AT slices for Perilipin/Dapi to determine fat cell areas, or Picrosirius red staining to visualize extracellular matrix deposition (Fig. 2A). Significantly less Picrosirius red labelling was detected in the ScAT of *Atg7 KO*^{PDGFRα} compared to control female mice (Fig. 2B), indicating that progenitors autophagy could

modulate fat tissue ECM deposition. We then examined ECM gene expression in different AT locations, namely the ScAT tissue of females and males, and the EpiAT of males. Significant reduction of the mRNAs encoding three fibrillary collagen alpha chains was consistently observed in *Atg7 KO*$^{PDGFR\alpha}$ compared to controls (Fig. 2C-E). The expression of several genes encoding other ECM components such as fibronectin, *Spp1* (secreted phosphoprotein 1 or osteopontin), or ECM modifying factors such as *Timp1* (Tissue inhibitor of metalloproteinase 1) and the collagen modifying lysyl oxidase genes (*Loxl1* and *Loxl2*) were also decreased in *Atg7 KO*$^{PDGFR\alpha}$ mice, with different intensities depending on the AT site (Fig. 2C-E). However, we found similar *Hif1a* and *Mmp2* mRNA in the ScAT of the two groups of mice (data not shown), although dysregulation of *Hif1a* or neutral matrix metalloproteases has been involved in AT fibrosis. We have also examined ECM gene expression in the ScAT of healthy mice fed chow, and confirmed that ECM genes were expressed at lower levels in control mice fed chow than in *Atg7*$^{lox/lox}$ mice fed HFD (Fig. S1A) indicating strong dependence of ECM gene regulation on diet/obesity. Moreover, ECM genes in ScAT of chow fed mice were expressed in the range of that found in *Atg7 KO*$^{PDGFR\alpha}$ mice fed HFD, suggesting that progenitor autophagy competency is required for ECM gene up-regulation by HFD.

Noticeably, AT ECM gene program attenuation in *Atg7 KO*$^{PDGFR\alpha}$ was observed in the hypotrophic ScAT of females (Fig. 2C) that contained smaller adipocytes (fig 2F), but also in the ScAT of males (Fig. 2D) that developed normally (Fig. 2G), although with a reduced number of fat cells (Fig. S1B). Reduction of Col3 gene expression was also found in the poorly developed EpiAT of males (Fig. 2E) that had normal-sized adipocytes (Fig. 2H). Moreover, at the end of the HFD, *Atg7 KO*$^{PDGFR\alpha}$ (both males and females) had lower body weights than controls (Fig. S2B), but only females had

significantly reduced fat mass (Fig. S2B). Triglyceride levels in serum of in the liver were not different in the two groups of mice (Fig. S2C), indicating that lower adiposity in autophagy deficient females was not compensated by ectopic lipid accumulation. This indicates that reduction of ECM gene expression not solely depends on site specific modulation of AT mass, fat cell size or adipocyte numbers. We also examined potential changes in local AT microenvironment that could modulate fibrogenic response, particularly AT inflammation. CD68, ADGRE1/Emr1, CD163, CD14 and CCL2/Mcp1 inflammation markers were not different in the subcutaneous fat of *Atg7 KO*$^{PDGFR\alpha}$ male or female versus respective *Atg7*$^{lox/lox}$ controls (Fig. S2A), indicating a minimal role of the inflammatory microenvironment. Thus, progenitor autophagy deficiency affects adipose tissue ECM gene program, independent on local fat tissue development and inflammation.

To further document contribution of progenitor autophagy, we next investigated ECM deposition driven by Pdgfrα^{+} AT progenitors that reside outside adipose tissue, for instance by Pdgfrα^{+} cells located in the sub-epicardial layer of the mouse atria (Fig. 3A) which provide a source for heart remodeling [12]. We established a fibrosis score using cardiac tissue staining with Masson's trichrome blue, which was defined as the proportion of atrial surface delineated with blue color (Fig. 3B, Table S1). A lower fibrosis score in hearts of HFD-fed *Atg7 KO*$^{PDGFR\alpha}$ compared to *Atg7*$^{lox/lox}$ control mice (Fig. 3C) indicated lower ECM deposition, as well as decreased epicardial AT accumulation (Fig. 3D). Gene expression of ECM markers was also lower in dissected atria of *Atg7 KO*$^{PDGFR\alpha}$ compared to *Atg7*$^{lox/lox}$ controls (Fig. 3E). Together these data indicate a role of autophagy in progenitor-driven matrix deposition following HFD, which is not limited to fat depots but also observed in cardiac progenitors.

Autophagy inhibition affects cell-autonomous ECM gene program linked to TGF-BMP pathway remodeling, independently of GTF2IRD1 and Mir29*.*

To demonstrate the causative effects of autophagy deficiency on ECM gene downregulation, we used a culture system of primary progenitors isolated from the stroma-vascular fraction of mouse subcutaneous fat, directly exposed to autophagy inhibitors, or to siRNA mediated *Atg7* knockdown. In this cell model, the lysosomal inhibitor Chloroquine (CQ) drastically decreased the expression of several collagen chain genes and remodeling enzymes as lysyl oxidase enzymes, fibronectin, and alpha actin (Fig. 4A). *Atg7* knock-down had similar effects (Fig. 4B), although less marked likely due to *Atg7* mRNA residual expression (15%). To gain insight into mechanisms, we reasoned that autophagy inhibition could exert anti-fibrotic effects by suppressing proteolytic clearance of an endogenous regulator of ECM gene program. Among negative factors whose accumulation could inhibit ECM gene expression, GTF2IRD1 was recently reported as an important transcriptional regulator in AT fibrosis [23], and therefore a good candidate mediator of anti-fibrotic effects of autophagy inhibition. Moreover, we found an amino-acid motif in the GTF2IRD1 protein sequence matching the consensus site of an LC3 interacting region (LIR) required for the taken up of cargos by autophagic vesicles, which suggests possible autophagy-dependent regulation of this factor (Fig. 4C). GTF2IRD1 protein readily accumulated in cells treated with chloroquine, as did the autophagosome marker LC3-II (Fig. 4D). Addition in the culture medium of pro-fibrotic TGFß reduced GTF2IRD1 content and this effect was abolished by lysosome inhibition (Fig. 4E). This is in agreement with a control of GTF2IRD1 protein content by autophagy. However, siRNA-mediated downregulation of GTF2IRD1 (Fig. 4F) was unable to obliterate chloroquine-induced inhibition of ECM genes (Fig. 4G), indicating that GTF2IRD1 is dispensable, and therefore not the

mediator of autophagy-dependent fibrotic gene inhibition. We next tested possible involvement of *Mir29*, another well-known inhibitor of ECM gene expression and tissue fibrosis [24]. We found no change in mir29 contents upon CQ treatment, despite efficient downregulation of *Col1a1* and *Col6a1* mRNA in CQ-treated cells, rulling out implication of mir29 (Fig. S3A).

A broader screen for genes involved in the TGF-BMP signaling pathway confirmed that most of them were detected and well expressed in our cell system. Forty two out of 86 genes were significantly (FDR<0.05) dysregulated in CQ-treated cells (Fig. S3B), among which previously observed downregulated *Col1a1* and *Col1a2* mRNA. Several additional genes encoding ECM components were found down-regulated in CQ-treated progenitors like *Dcn* (decorin) and *Thbs1* (thrombospondin 1) (Fig. S3C). Of note, a number of signaling components were dysregulated in cultured preadipocytes treated with CQ (Fig. 5A), including gene encoding secreted members of the Tgf/Bmp family such as *Fst* (follistatin), *Lefty* (Left-Right Deterrmination Factor), *Gdf5* (Growth and Differentiation Factor 5), *Gdf6,* and *Tgfb3* (Transforming Growth Factor Beta 3) that showed decreased expression compared to untreated cells. Not only paracrine members, but also genes encoding several surface receptors including *Acvr2 (*Activin A Receptor type2*)*, *Bmpr2* (Bome morphogenic receptor protein type2) were decreased by CQ treatment, as well as genes encoding intracellular signaling components of the TGF-BMP pathway including transcriptional regulators : *Smad2* and *Smad5* (SMAD family member 2 and 5). When presented as a correlation network to identify nodes with strongest associations (filter at p>0.997, absolute values) two groups of positively associated genes were identified, centered on core elements of the signaling machinery or on more accessory regulatory components, likely to drive observed changes (Fig. 5B). To explore the *in vivo* relevance of this finding from CQ

treated cells, we tested the expression of some of the most decreased genes in the ScAT of *Atg7 KO*$^{PDGFR\alpha}$ female mice with reduced fibrosis (Fig. 5C) or in cultured progenitors with Atg7 knock-down (Fig. 5D). We found downregulated *Fst, Lefty, Acvr2, and Bmpr2* mRNAs in Atg7 deficiency compared to respective control conditions. Furthermore, *Lefty* gene expression positively correlated with picrosirius staining in ScAT (Fig. 5E), which is in favor of a contribution of this gene product to ECM deposition. Altogether, we provide indication of profound remodeling of the pro- and anti-fibrotic gene expression landscape, and disruption of the balance of TGF-BMP family members in autophagy-deficient progenitors.

Atg7 deficiency in progenitors favors subcutaneous fat beigeing potential.

Surprisingly, our gene expression survey in autophagy-inhibited cultured preadipocytes also revealed stimulation of the transcriptional regulator PRDM3, a paralog of PRDM16, the master regulator of adipocyte beigeing (Fig. 5F). As PRDM3 was shown to be able to substitute PRDM16 for AT mitochondrial gene program regulation [25], this suggested a possible link between cell autonomous down-regulation of ECM gene program by autophagy inhibition and adipocyte beigeing. Furthermore, the possibility that adipose tissue beigeing in *Atg7 KO*$^{PDGFR\alpha}$ mice might contribute to their obesity resistant phenotype when fed a HFD led us to investigate adipose tissue browning in our model. ScAT mRNA expression of *Ucp1*, the canonical beige/brown marker mostly produced background amplification by RT-PCR, except in some samples which displayed a 10- to 100-fold expression range over background, here after referred to as *Ucp1*$^{+}$ (Fig. S4A). The gene expression of 2 other beige markers, *Tbx1* and *Ppargc1a* was also significantly higher in *Ucp1*$^{+}$ AT samples (Fig. S4B). Among 36 mice, we found that *Ucp1*$^{+}$ ScAT expression was more frequent in

Atg7 KO^{PDGFRα} mice than in controls (Fig. 5G, p=0.018, Fisher's exact test), suggesting that Atg7 deficiency in progenitors favors mice AT beigeing. We did not noticed any morphological indication of multilocular adipocytes in ScAT of these mice, however Ucp1 protein content tended to be higher (Fig. S4C). Of note, long-term HFD feeding and 22°C room temperature housing are minimally favorable environmental conditions for beige activation. Nevertheless, ScAT *Ucp1* mRNA expression negatively correlated with the expression of *Col1a1*, *Col3a1*, *Col6a1* and *Loxl2*, (Fig. 5H-I), indicating a link between autophagy-dependent ECM regulation and progenitor orientation. Thus, *Atg7 KO*^{PDGFRα} mice model complemented by *in vitro* studies established novel autophagy-dependent associations governed by progenitors phenotypes, inversely impacting beige conversion and ECM fibrotic remodeling.

Discussion:

PDGFRα expression delineates an heterogenous progenitor population with dual fibro/adipocyte potential, and constitutive PDGFRα activation was reported to switch progenitor cell fate towards fibrogenesis [8]. Here, we provide evidence that progenitor ECM gene response to obesogenic diet is impacted by autophagy ablation, and demonstrate cell-autonomous paracrine imbalance in the TGF-BMP pathway.

Our conclusion is based on the combination of experiments in a novel mice model with tamoxifen inducible *Atg7* gene targeting of PDGFRα+ cells, and cultured progenitors experiments with pharmacological or siRNA-mediated autophagy inhibition. We are aware of limitations on the mice model, related to the use of *Pdgfrα* promoter which is not strictly restricted to progenitors, leading to possible non-specific effects from targeting other cell types throughout the body. However, we show that PDGFRα is not expressed in the main cell types found in AT microenvironment like macrophages and

endothelial cells. Also, by including both males and females, we highlight sex- and depot- specific differences in *Pdgfr*α targeting efficiency among AT progenitors. This observation is currently unexplained, but can only minimize whole body phenotypic changes. Finally, due to the use of a tamoxifen inducible system, we cannot exclude that observed changes are drug-dependent, as tamoxifen is known to affect adipose tissue metabolism [26 ,27]. Particularly, tamoxifen can accumulate in the adipose tissue where it can cause adipocyte death and reversible lipoatrophy [28]. Thus, tamoxifen priming could influence subsequent responses to high fat diet by reducing progenitors survival to autophagy inhibition. However, in our model, we did not found decreased AT *Pdgfra* mRNA expression, that might be indicative of massive progenitor cell loss in autophagy-deficient mice (not shown). Despite model-dependent limitations, we believe that autophagy deficiency in progenitors is indeed the driver of AT changes reported here, because these can be reproduced *in vitro* in cultured autophagy-inhibited progenitors.

Our observation that autophagy-competent PDGFRα cells are required for HFD-induced AT fibrogenesis is reminiscent of a previous report in the liver, in which fibrosis was blunted by autophagy inhibition, although through a distinct mechanism [29]. In this liver study, blockade of stellate cells activation was related to inhibition of lipophagic degradation of preexisting intracellular retinol-esters stores, required for subsequent myofibroblast differentiation. So far, AT PDGFRα progenitors do not contain significant preexisting lipid stores, and we have no evidence that lipophagic degradation would be prerequisite for inhibition of ECM cell program. Rather, we demonstrated a cell-autonomous imbalance in the execution of gene program governing production and paracrine responsiveness of TGF-BMP factors, which is likely the cause of the decline of fibrogenic potential in autophagy deficient progenitors.

We point out a complex pathway comprising a large variety of paracrine/autocrine factors that interact with multiple receptor systems, which still needs to be investigated in more detail. Particularly, further studies will be required to elucidate autophagy-related transcriptional regulation of diverse TGF-BMP family members and their functional consequences. Noticeably, a recent study identified age-dependent modulation of dermal adipose progenitors fibrotic response by TGF-BMP factors, linked to progressive loss of their antimicrobial activity with advancing age [30]. Whether such age-dependent changes rely on autophagy modulation in dermal progenitors as described here for subcutaneous fat has not been investigated, but autophagic decline is a well-known feature in ageing. Also, related to TGF-BMP pathway, obesity can promote heart arrhythmias through fibrosis accumulation [31], and TGFb is up regulated in the atria of rats fed a HFD which favors fibrosis [32].

Single cell analysis tools are now becoming available to decipher cell heterogeneity within the adipose tissue progenitor population. From these experiments, coexistence of adipogenic progenitors with distinct non-adipogenic, regulatory subgroups of cells which can modulate adipose conversion through secreted factors has been identified [33, 34]. As PDGFRα expression is a common feature of all progenitors, and autophagy is an ubiquitous process, our functional targeting approach is likely to affect these populations unspecifically. However, selective responses of cell subtypes to autophagy inhibition cannot be excluded, ultimately affecting local TGF-BMP landscape. Interestingly, a recently published study identified TGFb as a modulator of progenitor sub-populations dynamics [35].

Beyond a primary role of progenitor autophagy status in fibrogenesis, our present data showing anti-adiposity effects of autophagy inhibition bring new insight in the control of beige/white adipogenesis (see [36] for recent review). The visceral fat phenotype of

male *Atg7 KO*$^{PDGFR\alpha}$ mice described here, namely the reduced fat pad weight along with unaffected fat cell size (see Fig. 2H) infers hypoplastic fat development. This is in agreement with studies where autophagy was inhibited in cultured cells, leading to drastic reduction of fat cell differentiation [37, 18]. Our study was designed to target adipose progenitors, whereas previous reports on autophagy inhibition have used an aP2 promoter [37, 18] which is only active in committed adipocytes. The common adipose tissue brown-like phenotype observed in the two systems indicates that autophagy-dependent regulations likely operate at two distinct steps in the process of beige adipocyte formation (ie. conversion from existing white fat cells, and *de novo* differentiation form progenitors). In the aP2 driven models, emergence of morphologic features of brown-like adipocytes would suggest favored conversion from white mature adipocytes, which is in agreement with the conclusions by [38], that limiting mitophagy, a specific form of autophagy could promote maintenance of differentiated brown-like fat cells overtime. In the present PDGFRα-driven model, as far as progenitors are primarily targeted, we suggest that autophagy can control the differentiation of beige adipocytes from dedicated precursors. Thus, similar to cold exposure, autophagy inhibition could orient progenitors towards preferential beige over white differentiation, even when applied in an obese setting. Whether this results from a shifted fate from white to beige of a common progenitor in early adipogenesis remains an opened question. However, we cannot completely exclude that modification of the secretory TGF-BMP landscape of autophagy deficient progenitors could induce local conversion from existing white to beige mature adipocytes. Globally, our study points to an anti-adiposity effect of progenitor autophagy inhibition, and suggests that mice can remain lean because white adipogenesis is impaired and brown-like fat cell formation is promoted.

Another interesting outcome of the present study is to highlight reciprocal links between AT beigeing and fibrogenesis. Although a progenitor switch between fibrogenic versus adipogenic development was previously documented [9], our data point to autophagy pathways as active modulators in this switch, and suggest that reciprocal relationships between the adipogenesis and fibrosis involve the “beige arm” of progenitor commitment. In agreement, a recent study in which beigeing stimuli were applied to lean mice fed a control diet reported decreased fibrotic phenotype of adipose precursors [39], a feature that declined with advancing age. Our data indicate that progenitor autophagy inhibition similarly favors beigeing and also minimizes adipose tissue fibrogenic potential, even in mice fed an obesogenic diet. The TGF pathway is a key actor in fibrogenesis, and some TGFb family members have been reported to modulate the development of beige adipocytes [40, 41], but it is still unclear how TGFb family members/receptor pathways govern this inverse relationship. There is clinical relevance in this question because acting on both AT fibrosis (an ultimate sign of dysfunction linked to insulin resistance) and AT browning (a favorable metabolic phenotype with positive effects on glucose utilization) would be expected to positively influence metabolic health when combined. The favorable phenotype of the *Atg7 KO*$^{PDGFR\alpha}$ mouse model with partial obesity resistance to HFD, no signs of liver alteration, preservation of AT beigeing potential and reduced fibrogenesis in subcutaneous fat and even in the pericardial region, suggests that autophagy inhibition might provide a basis for anti-fibrotic strategies in obesity.

Materials and Methods

Mice breeding.

All mice were housed in the animal facility of Pitié-Salpetrière, in conformity with EU regulations, and studied according a protocol that received ethics approval from the

French ministry for research (n° 01746.02). Floxed Atg7 founders were obtained as frozen embryos from Riken, (RBCC 02759 stock) and crossed to obtained $Atg7^{lox/lox}$ on a C57/Bl6J background. PDGFRα-Cre^{Ert2} transgenic animals were from Jackson Laboratory USA, Stock n° 018280). After DNA extraction, genotypes at the Atg7 and Cre loci were assessed as described by providers. *$Atg7^{lox/lox}$* and *$Atg7^{lox/lox}$-PDGFRa-Cre^{Ert2}* littermates were studied. All animals were housed in rooms with a 12 h-light cycle, genotyped before weaning, and littermates were matched according to sex and genotypes. At 4-6 weeks old (2-4 weeks post weaning) all animals received tamoxifen by 5 daily gavage (25 mg/ml in olive oil, 0.25 mg/g daily dose) and were subsequently fed a high fat diet (HFD, 60% cal from fat; Research diets, D12492i) for 10 weeks with free access to water. At the end of HFD-feeding, mice were analyzed for body composition by Nuclear Magnetic Resonance (Brucker Mini-spec plus), and then sacrificed by cervical dislocation between 9:00 and 11:00. Adipose tissues and liver were collected, snapped frozen or fixed in 4% formaldehyde for later analysis.

Adipose tissue histology.

Tissue sections were obtained from paraffin-embedded tissue and immunolabelled [42]. ImageJ software served to determine fat cell size by dividing total area of a given field by the number of adipocytes in the delimited area. At least 4 different random fields were quantified for each sample. Picrosirius red staining was performed as described previously [5].

Adipose tissue cell separation.

Collagenase (1 mg/ml; Sigma, 11088793001) was used to isolate adipose tissue cells as floating adipocytes or stroma-vascular fractions. After centrifugation stromal cells were sorted by FACS as described in Marcelin et al. [9]. Purified cell fractions were

frozen in RIPA (Sigma, R0278) or RLT buffer (Qiagen, 79216) for western blotting or RNA extraction respectively.

Epicardial fat studies.

Hearts were fixed in 4% paraformaldehyde and processed as described previously [12] to monitor the epicardial layer and fat. In 7-µm sections of mouse atria, an adipose tissue score was calculated based on the number of monolocular adipocytes infiltrating the epicardial layer in the atrial region (Table S1). A fibrosis score was also determined according to the fraction of epicardial layer with positive Masson's trichrome staining (Table S1). Frozen sections of atria were used for immunolabelling with anti-PDGFRa (Abcam) after DAPI counterstaining. Images were captured with Nikon NIS and analyzed with Image J software.

Western Blotting.

Adipose tissue extracts or isolated cell fractions were processed as described previously [43], with antibodies obtained from Cell Signaling Technology (ATG7, 2631; ACTB/ß-Actin, 4970; LC3, 4108), or Novus (GTF2IRD1, NBP1-91973). Linear range of signals were obtained by quantification of fluorescent secondary antibody with the Odyssey Imaging System (Licor).

RT-qPCR analysis.

mRNA was extracted from whole adipose tissue or cell fractions using a Qiagen kit. cDNA was reversed transcribed and real time q-PCR was performed using primer pairs validated for efficient amplification with serial cDNA dilutions. Gene expression was normalized to housekeeping genes (*Rna18s* or *Rplp0* mRNA) and relative values were calculated with the delta [delta Ct]) method. Expression of genes belonging to the TGF-

BMP signaling pathway were assessed by PCR Array (RT2 Profiler, Qiagen) following manufacturer instructions.

Cell culture.

Stroma vascular cells were isolated from inguinal subcutaneous adipose tissue of 8-10 weeks old mice and cultured in DMEM high glucose supplemented with antibiotics and 10% fetal calf serum (FCS). After 1-4 passages cells were plated in 6-well plates until 70% confluence and treated for 16 h in 1% FCS medium containing 25 µM chloroquine (Sigma, C6628) or 100 nM bafilomycin A_1 (Sigma, B1793). The effect of lysosomal inhibitors on autophagosome accumulation was assessed by western blot using LC3-II as an autophagosome marker. SiRNA transfection was performed with lipofectamine RNAiMAX (Invitrogen, 13778075) according to the manufacturer, with a pool of 3 100nM RNAi complexes from Origene, SR42185 (Gtf2ird1), SR427399 (Atg7), or SR30004 (scrambled controls). After 48 h-72 h RNA was extracted with RNeasy® mini Kit (Qiagen, 74104) and protein lysates were prepared in RIPA buffer.
In some experiments, stroma-vascular cell fraction obtained from human lipoaspirates was cultured in standard conditions and used to measure expression of *Mir29a* and *Mir29b*. RNA were extracted using miRNeasy mini kit (Qiagen, 217004), reversed transcribed with TaqMan™ Small RNA assay using specific primers (Applied Biosystem, RT002112 and RT000413) or RNU6B (RT001093) for normalization. Quantification was by qPCR with corresponding primers (Applied Biosystem, TM002112 and TM000413).

Statistical analysis.

Statistical significance was determined by two-tailed unpaired Wilcoxson-Mann-Whitney test on experimental groups comprising 8-12 age and sex-matched littermate mice. p values <0.05 were considered significant.

Disclosures. Funding from the French National Agency of research (ANR) is acknowledged and includes support from RHU collaborative grant CARMMA (15-RHUS-0003), from the Institute of Cardiometabolism and Nutrition (reference ANR-10-IAHU-05, to AL), ANR-14-CE12-0017-01 LIPOCAMD and ANR CAPTOR (ANR-17-CE14-0009). GM and KC also received funds from AFERO, EFSD-Novo Nordisk, and SFD to support for salaries and consumables. Authors have no competing interest to declare. We thank Pr Jean Christophe Bichet (Assistance Publique Hôpitaux de Paris, Pitié-Salpêtrière Hospital, Plastic surgery and Mammary Cancer Department) for providing lipoaspirates for human stromal cell fraction isolation. Timothy Swartz is acknowledged for language editing.

Reference List.

[1] M. S. Rodeheffer, K. Birsoy, and J. M. Friedman, “Identification of White Adipocyte Progenitor Cells In Vivo,” *Cell*, vol. 135, no. 2, pp. 240–249, 2008.

[2] H. K. Sung *et al.*, “Adipose vascular endothelial growth factor regulates metabolic homeostasis through angiogenesis,” *Cell Metab.*, vol. 17, no. 1, pp. 61–72, 2013.

[3] S. P. Weisberg, D. McCann, M. Desai, M. Rosenbaum, R. L. Leibel, and A. W. Ferrante, “Obesity is associated with macrophage accumulation in adipose tissue,” *J. Clin. Invest.*, vol. 112, no. 12, pp. 1796–1808, 2003.

[4] K. Sun, J. Tordjman, K. Clément, and P. E. Scherer, “Fibrosis and adipose tissue dysfunction,” *Cell Metab.*, vol. 18, no. 4, pp. 470–477, 2013.

[5] A. Divoux *et al.*, “Fibrosis in Human Adipose Tissue : Composition , Distribution , and Link With Lipid Metabolism and Fat,” *Diabetes*, vol. 59, pp. 2817–2825, 2010.

[6] P. B. Lassen *et al.*, “The fat score, a fibrosis score of adipose tissue: Predicting weight-loss outcome after gastric bypass,” *J. Clin. Endocrinol. Metab.*, vol. 102, no. 7, pp. 2443–2453, 2017.

[7] T. Iwayama *et al.*, “PDGFRalpha signaling drives adipose tissue fibrosis by targeting progenitor cell plasticity,” *Genes Dev*, vol. 29, no. 11, pp. 1106–1119, 2015.

[8] C. Sun, W. L. Berry, and L. E. Olson, “PDGFRα controls the balance of stromal and adipogenic cells during adipose tissue organogenesis,” *Development*, vol. 144, no. 1, pp. 83–94, 2017.

[9] G. Marcelin *et al.*, “A PDGFRα-Mediated Switch toward CD9highAdipocyte Progenitors Controls Obesity-Induced Adipose Tissue Fibrosis,” *Cell Metab.*, vol. 25, no. 3, pp. 673–685, 2017.

[10] Y. H. Lee, A. P. Petkova, E. P. Mottillo, and J. G. Granneman, “In vivo identification of bipotential adipocyte progenitors recruited by β3-adrenoceptor activation and high-fat feeding,” *Cell Metab.*, vol. 15, no. 4, pp. 480–491, 2012.

[11] R. Berry and M. S. Rodeheffer, “Characterization of the adipocyte cellular lineage in vivo,” *Nat. Cell Biol.*, vol. 15, no. 3, pp. 302–308, 2013.

[12] N. Suffee *et al.*, “Atrial natriuretic peptide regulates adipose tissue accumulation in adult atria,” *Proc. Natl. Acad. Sci. U. S. A.*, vol. 114, no. 5, pp. 771–780, 2017.

[13] I. K. Vila *et al.*, “Immune cell toll-like receptor 4 mediates the development of obesity- and endotoxemia-associated adipose tissue fibrosis,” *Cell Rep.*, vol. 7, no. 4, pp. 1116–1129, 2014.

[14] D. H. Madsen *et al.*, “M2-like macrophages are responsible for collagen degradation through a mannose receptor-mediated pathway,” *J. Cell Biol.*, vol.

202, no. 6, pp. 951–966, 2013.

[15] M. V. Plikus *et al.*, “Regeneration of fat cells from myofibroblasts during wound healing,” *Science (80-.).*, vol. 355, no. 6326, pp. 748–752, 2017.

[16] A. B. Novikoff, P. M. Novikoff, O. M. Rosen, and C. S. Rubin, “Organelle relationships in cultured 3T3-L1 preadipocytes,” *J. Cell Biol.*, vol. 87, no. 1, pp. 180–196, 1980.

[17] O. Pampliega *et al.*, “Functional interaction between autophagy and ciliogenesis,” *Nature*, vol. 502, no. 7470, pp. 194–200, 2013.

[18] R. Singh *et al.*, “Autophagy regulates adipose mass and differentiation in mice,” *J. Clin. Invest.*, vol. 119, no. 11, pp. 3329–3339, 2009.

[19] C. D. Church *et al.*, “Characterization of Cre recombinase models for the study of adipose tissue,” *Adipocyte*, vol. 3, no. 3, pp. 206–211, 2014.

[20] R. Singh *et al.*, “Autophagy regulates lipid metabolism,” *Nature*, vol. 458, no. 7242, pp. 1131–1135, 2009.

[21] B. Coupé, Y. Ishii, M. O. Dietrich, M. Komatsu, T. L. Horvath, and S. G. Bouret, “Loss of autophagy in pro-opiomelanocortin neurons perturbs axon growth and causes metabolic dysregulation,” *Cell Metab.*, vol. 15, no. 2, pp. 247–255, 2012.

[22] K. H. Kim *et al.*, “Autophagy deficiency leads to protection from obesity and insulin resistance by inducing Fgf21 as a mitokine,” *Nat. Med.*, vol. 19, no. 1, pp. 83–92, 2013.

[23] Y. Hasegawa *et al.*, “Repression of Adipose Tissue Fibrosis through a PRDM16-GTF2IRD1 Complex Improves Systemic Glucose Homeostasis,” *Cell Metab.*, vol. 27, no. 1, pp. 180-194.e6, 2018.

[24] B. Wang *et al.*, “Suppression of microRNA-29 Expression by TGF- 1 Promotes

Collagen Expression and Renal Fibrosis," *J. Am. Soc. Nephrol.*, vol. 23, no. 2, pp. 252–265, 2012.

[25] M. J. Harms *et al.*, "Prdm16 is required for the maintenance of brown adipocyte identity and function in adult mice," *Cell Metab.*, vol. 19, no. 4, pp. 593–604, 2014.

[26] L. Liu *et al.*, "Tamoxifen reduces fat mass by boosting reactive oxygen species," *Cell Death Dis.*, vol. 6, no. 1, pp. e1586-8, 2015.

[27] J. M. de Avila, M. Du, B. Wang, M.-J. Zhu, N. A. Gomez, and L. Zhao, "Even a low dose of tamoxifen profoundly induces adipose tissue browning in female mice," *Int. J. Obes.*, 2019.

[28] R. Ye *et al.*, "Impact of tamoxifen on adipocyte lineage tracing: Inducer of adipogenesis and prolonged nuclear translocation of Cre recombinase," *Mol. Metab.*, vol. 4, no. 11, pp. 771–778, 2015.

[29] V. Hernndezgea *et al.*, "Autophagy releases lipid that promotes fibrogenesis by activated hepatic stellate cells in mice and in human tissues," *Gastroenterology*, vol. 142, no. 4, pp. 938–946, 2012.

[30] L. Zhang *et al.*, "Age-Related Loss of Innate Immune Antimicrobial Function of Dermal Fat Is Mediated by Transforming Growth Factor Beta," *Immunity*, pp. 1–16, 2018.

[31] M. A. Pabon, K. Manocha, J. W. Cheung, and J. C. Lo, "Linking Arrhythmias and Adipocytes : Insights , Mechanisms , and Future Directions," vol. 9, no. December, pp. 1–12, 2018.

[32] T. Meng *et al.*, "Exposure to a chronic high-fat diet promotes atrial structure and gap junction remodeling in rats," *Int. J. Mol. Med.*, 2017.

[33] P. C. Schwalie *et al.*, "A stromal cell population that inhibit adipogenesis in

Mammalian Fat Depots," *Nature*, vol. 559, no. 7712, pp. 103–108, 2018.

[34] C. Hepler, L. Vishvanath, and R. K. Gupta, "Sorting out adipocyte precursors and their role in physiology and disease," *Genes and Development*, vol. 31, no. 2. pp. 127–140, 2017.

[35] D. Merrick *et al.*, "Identification of a mesenchymal progenitor cell hierarchy in adipose tissue," *Science (80-.).*, vol. 364, no. 6438, p. eaav2501, 2019.

[36] M. Shao *et al.*, "Cellular origins of beige fat cells revisited," *Diabetes*, vol. 68, no. 10, pp. 1874–1885, 2019.

[37] R. Baerga, Y. Zhang, P. H. Chen, S. Goldman, and S. Jin, "Targeted deletion of autophagy-related 5 (atg5) impairs adipogenesis in a cellular model and in mice," *Autophagy*, vol. 5, no. 8, pp. 1118–1130, 2009.

[38] S. Altshuler-Keylin *et al.*, "Beige Adipocyte Maintenance Is Regulated by Autophagy-Induced Mitochondrial Clearance," *Cell Metab.*, vol. 24, no. 3, pp. 402–419, 2016.

[39] W. Wang *et al.*, "A PRDM16-Driven Metabolic Signal from Adipocytes Regulates Precursor Cell Fate," *Cell Metab.*, vol. 30, no. 1, pp. 174-189.e5, 2019.

[40] U. D. Wankhade *et al.*, "TGF-β receptor 1 regulates progenitors that promote browning of white fat," *Mol. Metab.*, vol. 16, pp. 160–171, 2018.

[41] C. S. Craft *et al.*, "The extracellular matrix protein MAGP1 supports thermogenesis and protects against obesity and diabetes through regulation of TGF-β," *Diabetes*, vol. 63, no. 6, pp. 1920–1932, 2014.

[42] N. Briand, S. L. Lay, W. C. Sessa, P. Ferré, and I. Dugail, "Distinct roles of endothelial and adipocyte caveolin-1 in macrophage infiltration and adipose tissue metabolic activity," *Diabetes*, vol. 60, no. 2, pp. 448–453, 2011.

[43] H. Soussi *et al.*, “DAPK2 downregulation associates with attenuated adipocyte autophagic clearance in human obesity,” *Diabetes*, vol. 64, no. 10, pp. 3462–3463, 2015.

Figure legends.

Figure 1. Sex- and depot-specific efficiency of *Pdgfr*α promoter for AT progenitor targeting. (**A**) PDGFRα expression on cells from AT stroma-vascular fraction (SVF). Following collagenase digestion of AT, flow cytometry analysis was performed as described in [9], and PDGFRα expression was examined on 3 cell subsets: the endothelial cells (PECAM1/CD31^{+}), the leucocytes (PTPRC/CD45^{+}) and cells from SVF that do not expressed PECAM1 and PTPRC (PECAM1^{-} PTPRC^{-}). Here, we confirmed that PDGFRα, a marker of adipose progenitors, was not expressed in leucocytes or endothelial cells. (**B**) Using flow cytometry, the ratio of PDGFRA^{+} progenitors expressing Cre after tamoxifen gavage was evaluated in inguinal and perigonadal AT from females and males, based on fluorescent reporter protein expression. Mean values+/- sem are calculated from 4 cell preparations in each group. (**C**) Analysis of microarray data of FACS purified progenitors (PDGFRα+) from adipose tissue of fibrosis-proned C3H mice fed a HFD or a control chow diet for 8 weeks. A subset of autophagy-related gene is shown. (**D**) qPCR analysis of *Atg7* mRNA expression in AT FACS purified PDGFRα+ progenitors and macrophages. 1-2 AT were pooled for cell fractionation and subsequent RNA extraction. Data are expressed as the ratio of *Rna18s* normalized *Atg7* mRNA in *Atg7$^{lox/lox}$-Pdgfr*α *Cre*$^{+}$ versus matched *Atg7$^{lox/lox}$-Pdgfrα Cre-* littermates. (**E-F**) ATG7 and LC3 protein expression in subcutaneous adipose tissue of *Atg7 $^{lox/lox}$* and *Atg7 KO^{PDGFRα}* littermates, fed a HFD for 10 weeks. ßactin was used as a loading control. Representative western blots of

female ScAT (each lane is an individual mice) and densitometric quantification of signals after normalization to ACTB are shown.

Figure 2. *Progenitor Atg7 deficiency impacts adipose tissue ECM program.*

(A) Paraffin-embedded slides were immunolabelled with Perilipin/dapi, or stained with picrosirius red to image extracellular collagens. **(B)** After thresholding using ImageJ, picrosirius red label was quantified from five different fields per sample. Mean values were calculated from 6-9 mice per group, after adjusting for differences in fat cell area. **(C-E)** ECM-related gene expression in female mice ScAT (C) male mice ScAT (D) or male EpiAT (E). mRNA levels were normalized to 18S RNA. Values are mean ± sem from 9 mice per group. Symbols *, ** or *** indicate significant differences between groups of sex-matched littermates (by Mann-Whitney test) with $p < 0.05$, $p < 0.01$, or $p < 0.001$ respectively. **(F-H)** Fat pad weight and adipose cell size in AT depots (F: female mice ScAT; G: male mice ScAT; H: male mice EpiAT). Bars indicate mean values +/- sem of 6-9 individual animal per group. Fat pad weight is plotted on the left axis, and right axis is fat cell size, calculated from quantification of Perilipin/dapi images. P values by Man-Whitney tests are indicated when significant (<0.05).

Figure 3. *Progenitor Atg7 deficiency impacts ECM in heart atria.*

(A) PDGFRα immunostaining indicating presence of PDGFRα positive cells in the epicardic layer of heart atria. **(B)** blue Masson's trichrome staining of 7-µm sections of atria from male mice fed a HFD for 16 weeks. Scale bar = 50 µm, 100 µm. Morphological features of images served to calculate a fibrosis index **(C)** and epicardial AT score **(D)** in *Atg7*$^{lox/lox}$ mice (n=18, red dots) and *Atg7 KO*^{PDGFRα} mice (n=15, black dots). **(E)** ECM gene expression analysis in dissected mouse atria (7 mice per genotype). Relative gene expression is normalized to 18S, significant differences are indicated as *.

Figure 4. *Cell autonomous inhibition of collagen gene expression by autophagy inhibitors or siRNA-mediated Atg7 knock-down, dependence on GTF2IRD1.*

(A-B) Collagen gene expression in cultured preadipocytes treated for 16h with 25µM Chloroquine (A) or in Atg7 siRNA transfected cultured preadipocytes (B). **(C)** Alignment of mouse GTF2IRD1 protein sequence with the consensus motif for LC3 interaction. **(D-E)** GTF2IRD1 protein expression and quantification in cultured cells after chloroquine (D) or bafilomycinA_1 (E) treatment. **(F)** Inhibition of *Gtf2ird1* mRNA expression by siRNA in cultured preadipocytes from ScAT. **(G)** Collagen gene expression in cells transfected with *Gtf2ird1* siRNA or control siRNA, in the presence or absence of chloroquine (added one day post transfection for 16h). All values are means of at least three independent experiments. Stars indicate significant differences ($p<0.05$) by Student's t test.

Figure 5. *TGF-BMP family imbalance and AT browning after autophagy inhibition.*

(A) Change in *TGF-BMP* family members gene expression upon chloroquine treatment (16h) of cultured preadipocytes. Bars indicate fold change of mean values from three independent culture batches evaluated by PCR array. Colors indicate gene subgroups arranged by functional categories. **(B)** Correlation network established using qgraph R Package. Nodes with correlation coefficients above a threshold ($p>0.997$, absolute values) with positive (blue), or negative (red) association are shown. **(C)** Gene expression in the ScAT of female *Atg7 KO* $^{PDGFR\alpha}$ or *Atg7* $^{lox/lox}$ control mice. Bars are mean values ± sem of 8 individual mice in each groups. P values are indicated. **(D)** Relative mRNA expression in siRNA-mediated *Atg7* invalidation in cultured ScAT preadipocytes. Mean values +/- sem are calculated from 3 independent cell preparations. **(E)** Spearman correlation linking *Lefty* gene expression and ECM deposition by picrosirius red staining. **(F)** Change in *Prdm3* mRNA expression after

16h-chloroquine exposure of preadipocytes. Significant difference by t test is indicated as *. **(G)** Stratification of mice (36 in total) across AT *Ucp1* mRNA expression and genotype. **(H-I)** Significant Spearman's correlations with ScAT *Ucp1* mRNA expression.

Figure 1

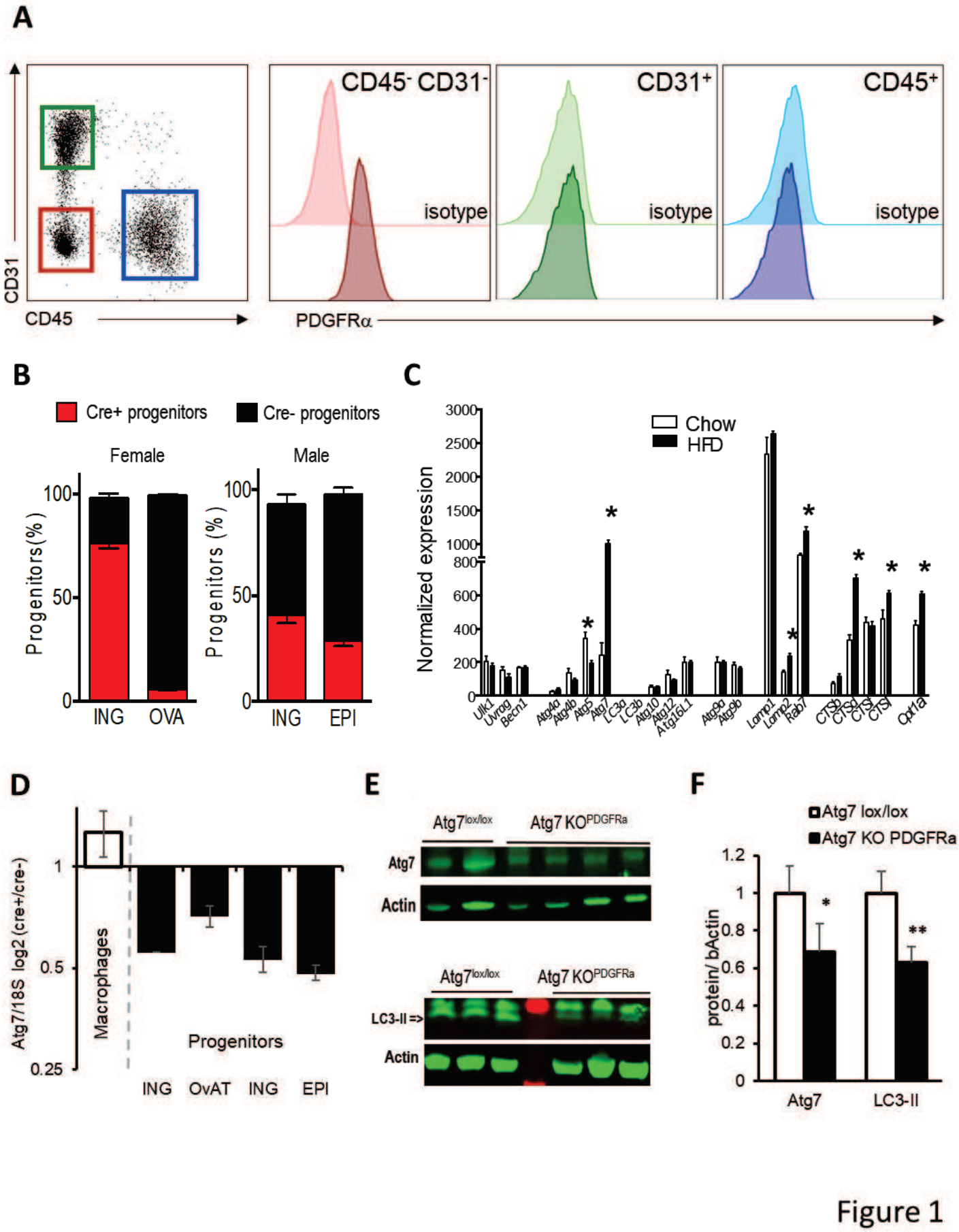

Figure 1

Figure 2

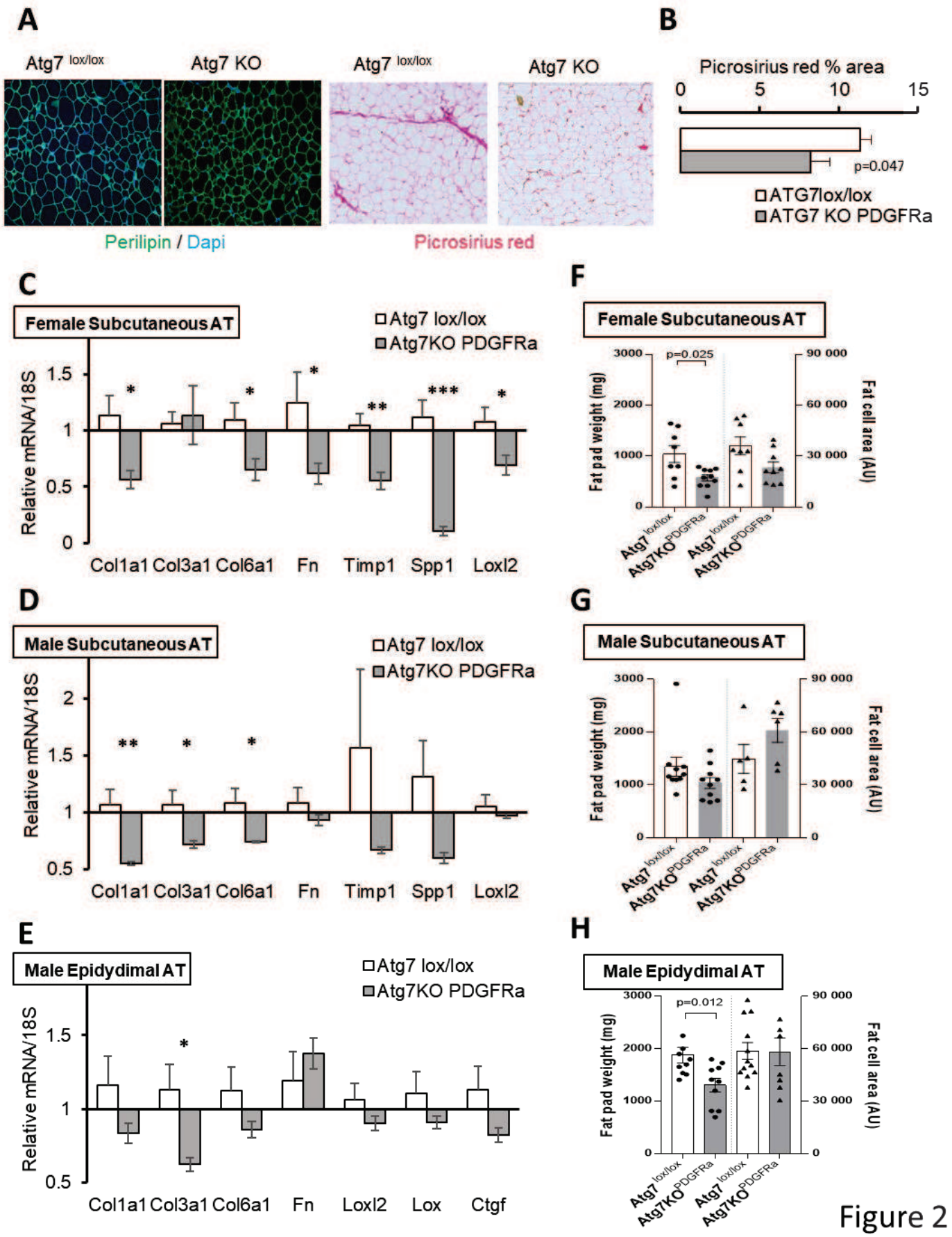

Figure 2

Figure 3

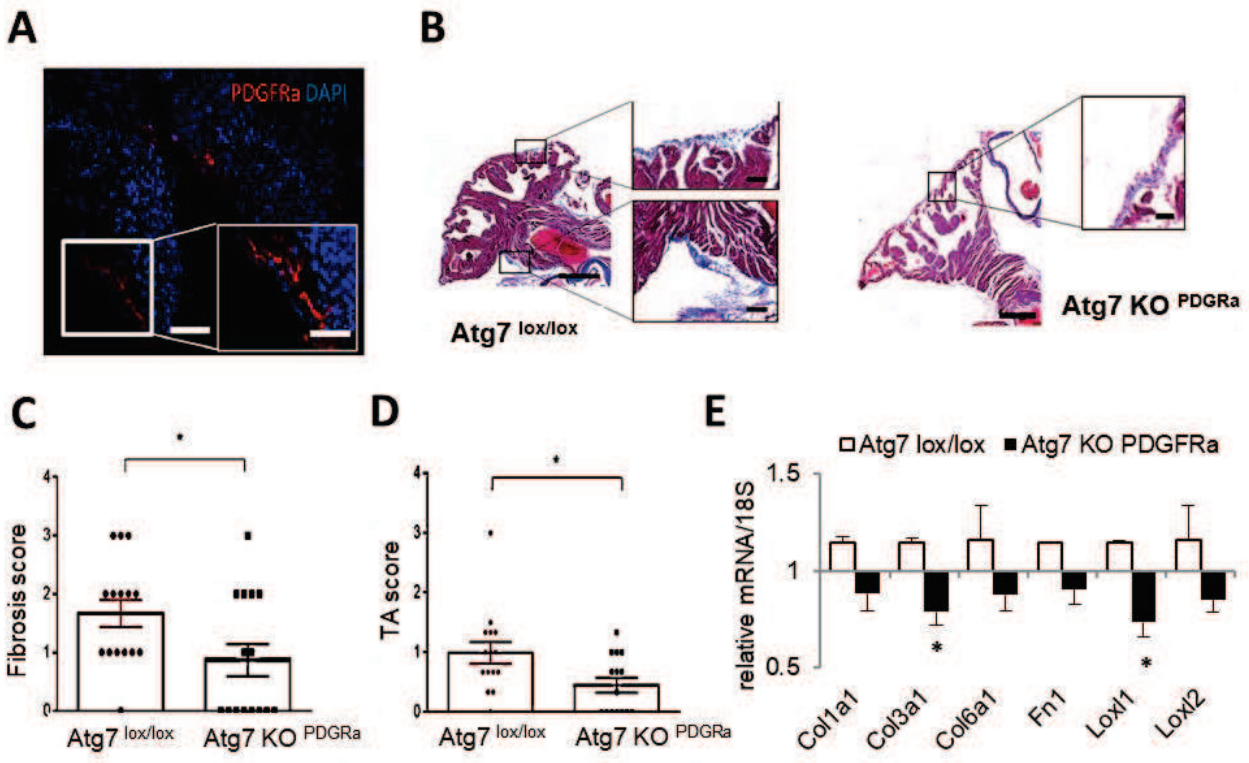

Figure 3

Figure 4

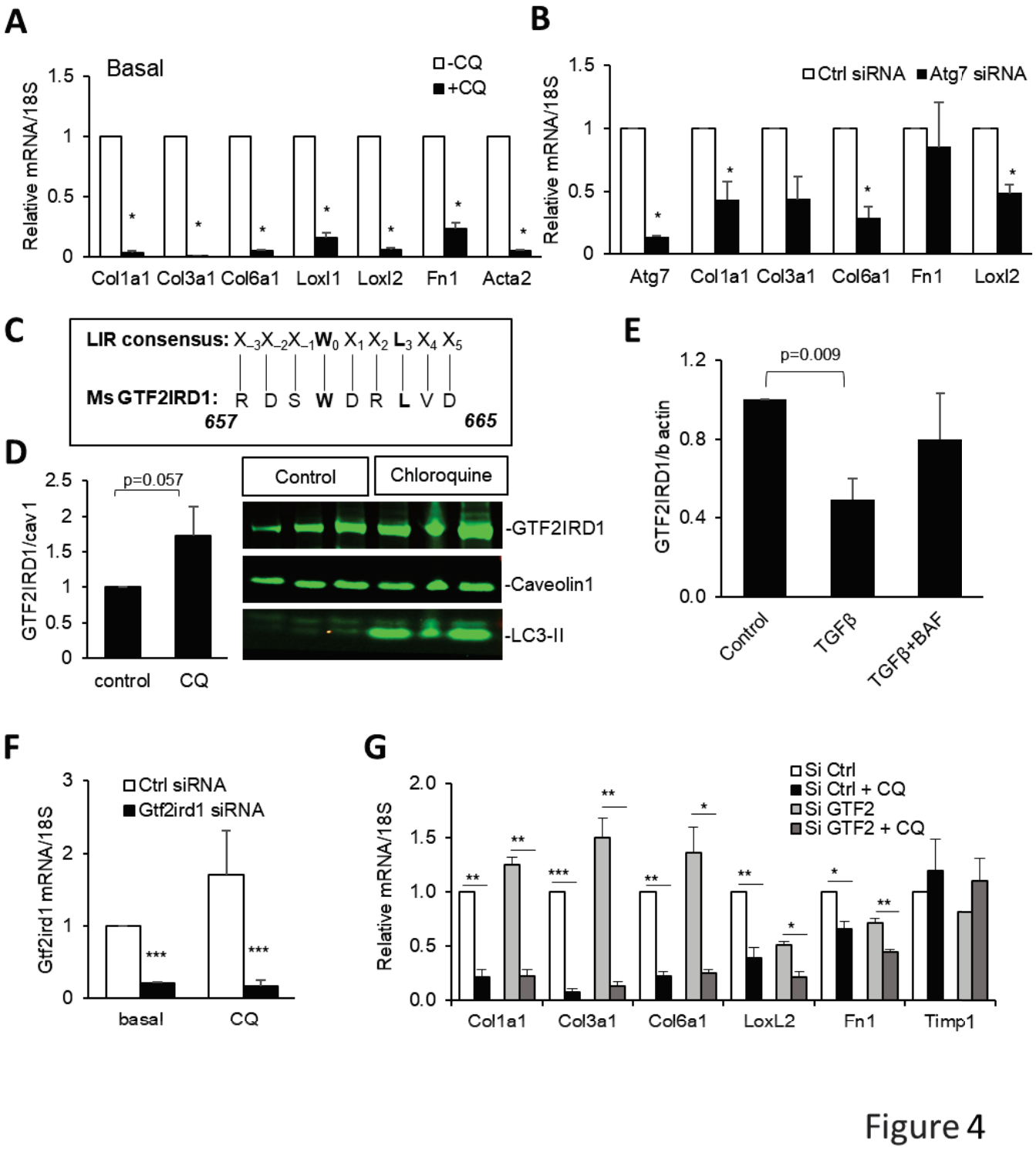

Figure 4

Figure 5

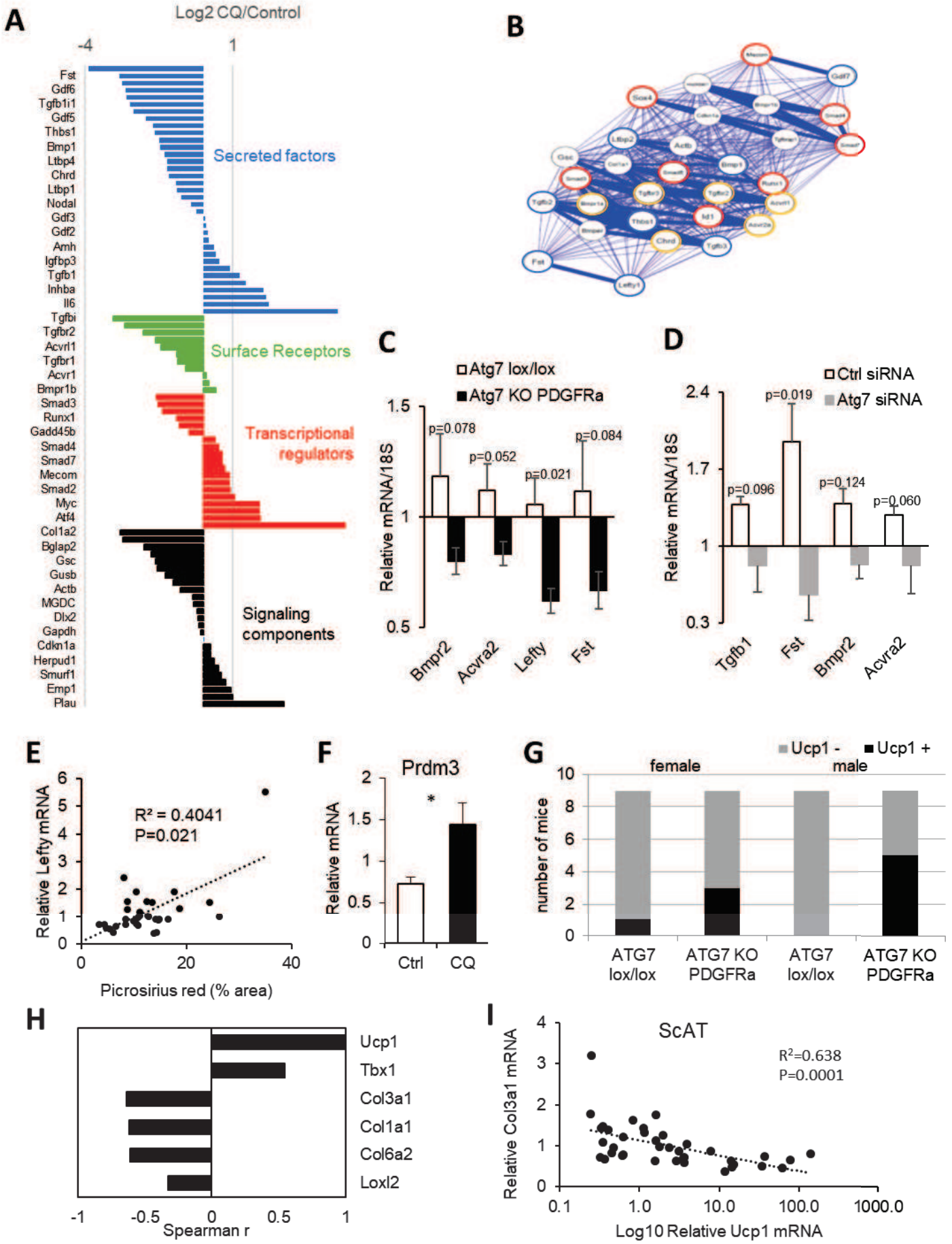

Figure 5